Journal of the Brazilian Society of Mechanical Sciences and Engineering (2019) 41:518
https://doi.org/10.1007/s40430-019-2005-3

TECHNICAL PAPER

Numerical solution for flow of a Eyring–Powell fluid in a pipe with prescribed surface temperature

Mubbashar Nazeer[1] · **Fayyaz Ahmad**[3] · **Mubashara Saeed**[1] · **Adila Saleem**[1] · **Sidra Naveed**[1] · **Zeeshan Akram**[2]

Received: 24 January 2019 / Accepted: 26 September 2019 / Published online: 30 October 2019

Abstract

In the current study, the flow and heat transfer of MHD Eyring–Powell fluid in a circular infinite pipe is discussed. The rheology of fluid is described by constitutive equation of Eyring–Powell fluid. The solution is constructed for both constant and variable viscosity cases. For variable viscosity case, the viscosity function is defined by Reynolds and Vogel's models. The solution of each case is calculated numerically with the help of eminent iterative numerical technique. The effects of thermo-fluidic parameters on flow and heat transfer phenomenon are highlighted through graphs. The velocity and temperature profiles diminish against magnetic parameter (M_e) and material parameter (M) in all cases, whereas both velocity and temperature profiles rise via magnitude of the pressure gradient and material parameter Y. The validity of our numerical results due to shooting method is presented by comparing them with the numerical results produced by pseudo-spectral collocation method. Relative absolute errors are plotted, and achieved accuracies are of the order four and five in w and θ, respectively. The outcomes of current investigation may be useful in thin film, catalytic reactors, polymer solutions and paper production, etc.

Keywords Variable viscosity · Eyring–Powell fluid · Pressure driven flow · Shooting method

1 Introduction

The non-Newtonian fluid has various applications in science and technology [1–3]. Theoretical studies give the important information related to investigation and modeling of mass and energy transfer in non-Newtonian fluids [4–6]. Generally, the flow behavior of non-Newtonian fluids is much complex as compare to Newtonian fluids. Non-Newtonian fluids such as polymeric solutions, muddy, coal-water, inks, blood and oils [7–9] contained a nonlinear relationship between viscous shear stress and velocity gradient. Such type of fluids is generally used in chemical and polymer processing, namely bubbles absorption, composite and molten plastic foam processing, etc. Rheological features of non-Newtonian fluids are commonly used in biomedical and biological devises. Generally, non-Newtonian fluid models lead the constitutive nonlinear stress–strain relation, which lead the nonlinear equations of motion. It is clearly noted that non-Newtonian fluids model cannot be addressed by a single constitutive equation between shear rate and shear stress. Due to such reason, some famous non-Newtonian models proposed by various authors such as: Akbar et al. [10] used the asymmetric channel for the peristaltic flow of Williamson nano-fluid. They used fifth-order Runge–Kutta–Fehlberg method to solve the nonlinear differential equations and presented some important results in the form of streamlines, velocity and temperature profiles. Slips effects on peristaltic flow of Jeffery's fluid in an asymmetric channel were discussed by Akbar and Nadeem [11]. They concluded that the pressure is an increasing function of Hartmann number, perturbation, thermal slip and relaxation parameter. Ellahi [12] examined the slip effects on Oldroyd eight constant fluid in a channel, and Homotopy analysis method was implemented to solve the nonlinear boundary value problem. Analytical study of flow of Casson fluid over

Technical Editor: Cezar Negrao, PhD.

Mubbashar Nazeer
mubbashariiui@gmail.com

[1] Department of Mathematics, Riphah International University Faisalabad Campus, Faisalabad 38000, Pakistan

[2] Department of Mathematics, Minhaj University Lahore, Lahore, Pakistan

[3] Department of Mathematics, National Textile University Faisalabad Campus, Faisalabad 38000, Pakistan

an exponentially shrinking sheet under the effects of magnetic field was investigated by Nadeem et al. [13]. Alamri et al. [14] used the Cattaneo–Christov heat flux model in the flow of second grade fluid over a stretching cylinder to explores the heat transfer characteristics. The effects of inclined magnetic field and heat transfer analysis on peristaltically induced motion of particle through uniform channel were analyzed by Bhatti et al. [15]. The effects of mass and bioheat transfer on MHD two-phase Sisko fluid inside the porous channel were determined by Bhatti et al. [16]. They used the homotopy perturbation method to find the series solution of the modeled equations. Ellahi et al. [17] investigated the combined effects of slip and entropy generation on MHD boundary layer flow over a moving plate. Hassan et al. [18] utilized the Dupuit–Forchheimer and Darcy's law models for the investigation of heat transfer phenomena of nano-fluid in a porous wavy surface. Effects of magnetic dipole and suction on the viscoelastic fluid over a stretching sheet were explored by Majeed et al. [19]. A numerical investigation of free convection flow inside a porous inclined rectangular conduit under the effect of surface radiation was analyzed by Shirvan et al. [20]. They employed finite volume method for the solution of couple nonlinear partial differential equations. Hassan et al. [21] obtained the analytical expression of velocity and temperature profiles for Cu–Ag/water hybrid nanofluids inside the inverted cone. Yousaf et al. [22] performed the shooting method for the study of thermal boundary layer flow of non-Newtonian fluid over an exponentially permeable stretching sheet.

Extensive literature can be seen in which many models have been proposed to account the viscosity's dependence on temperature of the fluid. For this, there are two famous models are noted in the literature, namely Reynolds and Vogel's models. Some, useful studies on variable viscosity models are presented in the next paragraph.

Turkyilmazoglu [23, 24] used the variable physical properties to account the magnetic and thermal radiation effects over rotating porous body. Bhatti et al. [25] examined the effects of slip condition and variable viscosity on clot blood model. Ellahi and Riaz [26] investigated the effects of variable properties on third-grade fluid in a pipe and presented the explicit analytical solution of the problem. In another study, Ellahi [27] examined the effects of magnetohydrodynamic flow of third-grade fluid inside the tube under the different viscosity models. He used the homotopic analysis method to predict the important results.

Power-law model is mostly use to predict the behavior of non-Newtonian fluids. Mathematically, the power-law model looks like simple model but having some restriction over Eyring–Powell fluids. In modern era, numerous researchers have used the Powel-Eyring fluid model and illustrated the various aspects. For this, Hayat et al. [28] used the series solution method to find the solution of nonlinear modeled equations of Eyring–Powell fluid and highlighted the important results. Hayat et al. [29] analyzed the effects of magnetic field, heat generation/absorption and thermal radiation on Eyring–Powell fluid over a stretching cylinder. Finite difference numerical technique was performed by Akbar et al. [30] to capture the effects of magnetic field on flow of Eyring–Powell fluid over a stretching surface. Nadeem and Saleem [31] employed the optimal homotopy analysis method to solve the nonlinear partial differential equations of Eyring–Powell fluid model and pointed out some useful results. The effects of physical parameters on MHD Eyring–Powell fluid over a rotating surface were investigated by Khan et al. [32]. Hayat et al. [33] applied the homotopy approach for the investigation of Eyring–Powell fluid over a stretching sheet under the effects of Brownian motion and magnetic field.

According to Ellahi et al. [34], the non-Newtonian fluid models are divided into three different classes, namely integral, rate types and differential. The Eyring–Powell fluid model has certain advantages over other non-Newtonian models like Power-law model because it shows Newtonian behavior against low and high shear rates. The Eyring–Powell fluid model is derived from kinematic theory rather than empirical relation, due to this reason it is favorite over other non-Newtonian fluid models. Such model characterizes the behavior of viscoelastic suspension and polymeric solutions against extensive ranges of shear rates. In the present study, the Eyring–Powell fluid inside the pipe under the effects of magnetic field is incorporated. To our best knowledge, there is no investigation available that deals with the flow of temperature dependent Eyring–Powell fluid in a pipe. Such type of flow configuration is commonly used in polymeric liquids, slurries and food stuffs, etc. [35]. In this investigation, the motivation emanates from a desire to realize the effects of magnetic field on Eyring–Powell fluid in a pipe. The shooting method based on Newton method [36, 37] is implemented to find the solution of considered problem. The important results of present study are highlights with the help of plots.

2 Problem formulation

Let us consider the steady-state fully developed, incompressible one-dimensional MHD flow of Eyring–Powell fluid inside a pipe. It is assumed that the fluid is flowing inside the pipe is electrical conducting fluid with applied uniform magnetic field $\boldsymbol{B}_0$. Further, we have neglected the electric and induced magnetic. The fluid flow inside the pipe is due to constant pressure gradient. The geometry of the present problem is shown in Fig. 1. However, here the rheology of fluid flowing in the pipe is characterized by Erying–Powell

Fig. 1 Geometry of the considered study

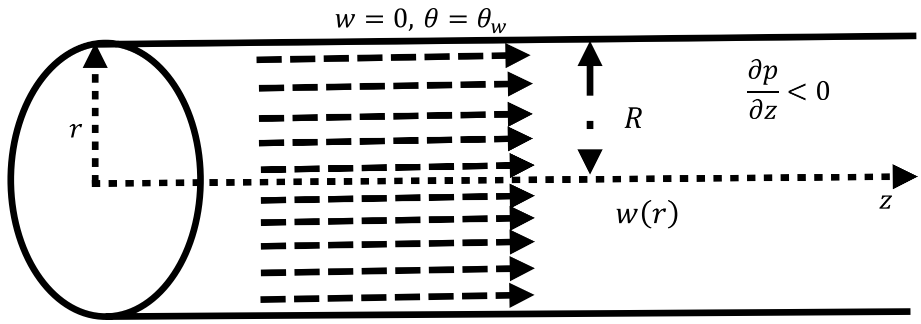

model. In particular, the analysis is carried out for three different viscosity models.

The Cauchy-stress tensor for the current study is [38]

$$\mathbf{S} = \left[\mu + \frac{1}{K_2}\frac{\mathrm{Sinh}^{-1}(K_3\dot{\psi})}{\dot{\psi}}\right]\mathbf{A}_1, \quad \text{where} \quad \dot{\psi} = \sqrt{\frac{1}{2}\mathrm{tra}(\mathbf{A}_1^2)}. \tag{1}$$

Powell and Erying [38] present the relation given in Eq. (1). With the help of Sinh^{-1} approximation

$$\mathrm{Sinh}^{-1}(K_3\dot{\psi}) \cong K_3\dot{\psi} - \frac{1}{6}(K_3\dot{\psi})^3, \quad |K_3\dot{\psi}| \ll 1. \tag{2}$$

The new form of Eq. (1) is

$$\mathbf{S} = \left[\mu + \mathrm{A} - \frac{B}{6}\dot{\psi}^2\right]\mathbf{A}_1, \quad B \ll 1, \tag{3}$$

where $A = \frac{K_3}{K_2}$ and $B = \frac{K_3^3}{K_2}$.

The velocity and temperature fields are defined by the given expression

$$\mathbf{V} = [0, 0, w(r)], \tag{4}$$

$$\theta = \theta(r). \tag{5}$$

In view of Eq. (4), the stress tensor has the following form

$$\mathbf{S} = \left(\mu + A - \frac{B}{6}\left(\frac{\mathrm{d}w}{\mathrm{d}r}\right)^2\right)\begin{pmatrix} 0 & 0 & \left(\frac{\mathrm{d}w}{\mathrm{d}r}\right) \\ 0 & 0 & 0 \\ \left(\frac{\mathrm{d}w}{\mathrm{d}r}\right) & 0 & 0 \end{pmatrix}. \tag{6}$$

It is noted that from above equation, $S_{rz}(S_{zr})$ only non-vanishing components of stress tensor $\mathbf{S}$

$$S_{rz} = S_{zr} = \left(\mu + A - \frac{B}{6}\left(\frac{dw}{dr}\right)^2\right)\left(\frac{dw}{dr}\right). \tag{7}$$

In the present situation, equations of continuity and conservation of momentum are given by

$$\frac{\partial w}{\partial z} = 0, \tag{8}$$

$$0 = -\frac{\partial p}{\partial z} + \frac{1}{r}\frac{\partial}{\partial r}(rS_{rz}) - \sigma B_0 w, \tag{9}$$

Substituting the values S_{rz} into Eq. (9), we have

$$\frac{1}{r}\frac{\mathrm{d}}{\mathrm{d}r}\left(\mu r\frac{\mathrm{d}w}{\mathrm{d}r}\right) + \frac{1}{r}\frac{\mathrm{d}}{\mathrm{d}r}\left(r\left(A\frac{\mathrm{d}w}{\mathrm{d}r} - \frac{B}{6}\left(\frac{\mathrm{d}w}{\mathrm{d}r}\right)^3\right)\right) - \sigma B_0 w = \frac{\mathrm{d}p}{\mathrm{d}z}. \tag{10}$$

The energy equations in the present problem take the following form:

$$\frac{\mu}{k}\left(\frac{\mathrm{d}w}{\mathrm{d}r}\right)^2 + \frac{A}{k}\left(\frac{\mathrm{d}w}{\mathrm{d}r}\right)^2 - \frac{B}{6k}\left(\frac{\mathrm{d}w}{\mathrm{d}r}\right)^4 + \frac{\mathrm{d}^2\theta}{\mathrm{d}r^2} + \frac{1}{r}\frac{\mathrm{d}\theta}{\mathrm{d}r} = 0. \tag{11}$$

The boundary conditions of Eqs. (10) and (11) are

$$w = 0, \quad \theta = \theta_w, \quad \text{at} \quad r = R, \quad \text{and} \quad \frac{\mathrm{d}w}{\mathrm{d}r} = \frac{\mathrm{d}\theta}{\mathrm{d}r} = 0 \quad \text{at} \quad r = 0. \tag{12}$$

With the help of normalized quantities [4], the new form of Eqs. (10)–(12) are:

$$\frac{1}{\bar{r}}\frac{\mathrm{d}}{\mathrm{d}\bar{r}}\left(\bar{\mu}\bar{r}\frac{\mathrm{d}w}{\mathrm{d}\bar{r}}\right) + \frac{1}{\bar{r}}\frac{\mathrm{d}}{\mathrm{d}\bar{r}}\left(\bar{r}\left(A\frac{\mathrm{d}\bar{w}}{\mathrm{d}\bar{r}} - \frac{B}{6}\left(\frac{\mathrm{d}\bar{w}}{\mathrm{d}\bar{r}}\right)^3\right)\right) - M_e^2\bar{w} = C, \tag{13}$$

$$\frac{\mathrm{d}^2\bar{\theta}}{\mathrm{d}\bar{r}^2} + \frac{1}{\bar{r}}\frac{\mathrm{d}\bar{\theta}}{\mathrm{d}\bar{r}} + \frac{\bar{\mu}}{k}\left(\left(\frac{\mathrm{d}\bar{w}}{\mathrm{d}\bar{r}}\right)^2 + \frac{A}{\bar{\mu}}\left(\frac{\mathrm{d}\bar{w}}{\mathrm{d}\bar{r}}\right)^2 - \frac{B}{6\bar{\mu}}\left(\frac{\mathrm{d}\bar{w}}{\mathrm{d}\bar{r}}\right)^4\right) = 0, \tag{14}$$

$$\bar{w} = 0, \quad \bar{\theta} = 0 \quad at \quad \bar{r} = 1, \quad and \quad \frac{d\bar{w}}{d\bar{r}} = \frac{d\bar{\theta}}{d\bar{r}} = 0 \quad at \quad \bar{r} = 0. \tag{15}$$

where $M_e^2 = {\sigma B_0 R}/{\mu_0}$ is the magnetic parameter.

It is noted that the momentum equation will be different against different viscosity models such form is defined separately in separate section.

2.1 Constant viscosity model

For this case, $\bar{\mu} = 1$, and Eq. (13) becomes

$$\frac{\mathrm{d}}{\mathrm{d}\bar{r}}\left(\bar{r}\frac{\mathrm{d}\bar{w}}{\mathrm{d}\bar{r}}\right) + M\frac{\mathrm{d}}{\mathrm{d}\bar{r}}\left(\bar{r}\left(\frac{\mathrm{d}\bar{w}}{\mathrm{d}\bar{r}}\right)\left(1 - \chi^*\left(\frac{\mathrm{d}\bar{w}}{\mathrm{d}\bar{r}}\right)^2\right)\right) = \bar{r}(C + M_e^2\bar{w}), \tag{16}$$

where $M = \frac{A}{\mu_0}$, $\chi^* = \frac{K_3^2 w_0^2}{6\mu_0 R^2}$.

2.2 Reynold's model

According to this model $\mu(\theta) = \mu_0 e^{-n\theta}$ therefore $\bar{\mu} = e^{-n\theta_w} e^{-L\bar{\theta}}$ and

$$e^{-L\bar{\theta}} \frac{1}{\bar{r}} \frac{\mathrm{d}}{\mathrm{d}\bar{r}} \left(\bar{r} \frac{\mathrm{d}\bar{w}}{\mathrm{d}\bar{r}} \right) - L e^{-L\bar{\theta}} \frac{\mathrm{d}\bar{\theta}}{\mathrm{d}\bar{r}} \frac{\mathrm{d}\bar{w}}{\mathrm{d}\bar{r}} + \frac{M}{\bar{r}} \frac{\mathrm{d}}{\mathrm{d}\bar{r}} \left(\bar{r} \left(\frac{\mathrm{d}\bar{w}}{\mathrm{d}\bar{r}} - \chi^* \left(\frac{\mathrm{d}\bar{w}}{\mathrm{d}\bar{r}} \right)^3 \right) \right) - M_e^2 \bar{w} = C, \tag{17}$$

where $\chi^* = \frac{K_3^2 w_0^2}{6\mu^* R^2}$ and $\mu^* = \mu_0 e^{-n\theta_w}$. For this case λ in Eq. (11) is defined by $\lambda = \mu^* w_0^2 / k(\theta_m - \theta_w)$.

2.3 Vogel's model

For this model $\mu(\theta) = \mu_0 e^{\left(\frac{X}{Y+\bar{\theta}}\right)}$ or $\bar{\mu} = e^{\theta_w} e^{\left(\frac{X}{Y+\bar{\theta}} - \theta_w\right)}$. Thus dimensionless equation of motion in this case is

$$e^{\left(\frac{X}{Y+\bar{\theta}} - \theta_w\right)} \frac{1}{\bar{r}} \frac{\mathrm{d}}{\mathrm{d}\bar{r}} \left(\bar{r} \frac{\mathrm{d}\bar{w}}{\mathrm{d}\bar{r}} \right) - \frac{X}{(Y+\bar{\theta})^2} e^{\left(\frac{X}{Y+\bar{\theta}} - \theta_w\right)} \frac{\mathrm{d}\bar{\theta}}{\mathrm{d}\bar{r}} \frac{\mathrm{d}\bar{w}}{\mathrm{d}\bar{r}} + \frac{M}{\bar{r}} \frac{\mathrm{d}}{\mathrm{d}\bar{r}} \left(\bar{r} \left(\frac{\mathrm{d}\bar{w}}{\mathrm{d}\bar{r}} - \chi^* \left(\frac{\mathrm{d}\bar{w}}{\mathrm{d}\bar{r}} \right)^3 \right) \right) - M_e^2 \bar{w} = C, \tag{18}$$

where $\mu^* = \mu_0 e^{\theta_w}$.

The boundary conditions of Eqs. (16)–(18) are

$$\bar{w} = 0 \quad \text{at} \quad \bar{r} = 1, \quad \text{and} \quad \frac{\mathrm{d}\bar{w}}{\mathrm{d}r} = 0 \quad \text{at} \quad \bar{r} = 0. \tag{19}$$

The shooting method is selected for the solution of the given boundary value problems. The detail of shooting method is present in the next section.

3 Numerical solution

It is noted that the analytical solution of each system in each case is not possible due to nonlinearity and coupling appear in each equation. Due to this reason, the boundary value problem of an ordinary differential equations is solved with numerical technique (shooting method). Various techniques have been implemented to obtain the solution of complex rheological models which are cited in introduction section. The main problem noted with such type of techniques is that when you discretize the differential equations into system of algebraic equations it is time consuming and we get highly nonlinear algebraic structure. Particularly, it takes penalty of time when we enhance the interval and number of mesh points to attain the accuracy. The shooting method based on Runge–Kutta scheme of order 4 combined with Newton–Raphson's method, based on step-by-step technique in which we use previous solution to approximate the next one. In this scheme, all the differential equations have unit order. This numerical scheme is very eminent, less time consuming, stable and rapidly convergent as explained in [39–50]. In some cases, when we have physical constraints on dependent variable, the iterative numerical solution of discretized nonlinear boundary value problems by using Newton–Raphson method is divergent. In this scenario, we prefer to use shooting method. The graphical results and discussion are given in next section. The flowchart is presented below to show the short view of this method that how to work this method. For the employment of the shooting method, first of all we want to transform the achieved system of equation of the constant viscosity case, such as

$$\frac{\mathrm{d}\bar{w}}{\mathrm{d}\bar{r}} = \bar{f}_1, \tag{20}$$

$$\frac{\mathrm{d}^2\bar{w}}{\mathrm{d}\bar{r}^2} = \frac{\mathrm{d}\bar{f}_1}{\mathrm{d}\bar{r}}, \tag{21}$$

$$\frac{\mathrm{d}\bar{\theta}}{\mathrm{d}\bar{r}} = \bar{f}_2, \tag{22}$$

$$\frac{\mathrm{d}^2\bar{\theta}}{\mathrm{d}\bar{r}^2} = \frac{\mathrm{d}\bar{f}_2}{\mathrm{d}\bar{r}}. \tag{23}$$

$$\frac{\mathrm{d}\bar{f}_1}{\mathrm{d}\bar{r}} = \frac{\left[\bar{r}\left(C + M_e^2 \bar{w}\right) + M\chi^* \bar{f}_1^3 - (1+M)\bar{f}_1\right]}{\bar{r}\left[(1+M) - 3M\chi^* \bar{f}_1^2\right]}, \tag{24}$$

$$\frac{\mathrm{d}\bar{f}_2}{\mathrm{d}\bar{r}} = -\left[\frac{\bar{f}_2}{\bar{r}} + \lambda \bar{f}_1^2 \left(1 + M - M\chi^* \bar{f}_1^2\right)\right], \tag{25}$$

$$\bar{w}(0) = k, \quad \bar{f}(0) = 0, \quad \bar{\theta}(0) = l, \quad \bar{g}(0) = 0. \tag{26}$$

In above (26), k and l represent the unknown slopes (missing conditions) and these are pick as boundary conditions at unity are fulfilled. In the numerical implementation of shooting method, we face singularity at $\bar{r} = 0$. In fact, we need $\bar{w}''(0)$ and $\bar{\theta}''(0)$ to start Runge–Kutta fourth-order method. By using L'Hospital's rule, we computed the values of

$$\bar{w}''(0) = \frac{M_e^2 \bar{w}_0 + C}{2(1+M)}, \tag{27}$$

and

$$\bar{\theta}''(0) = 0. \tag{28}$$

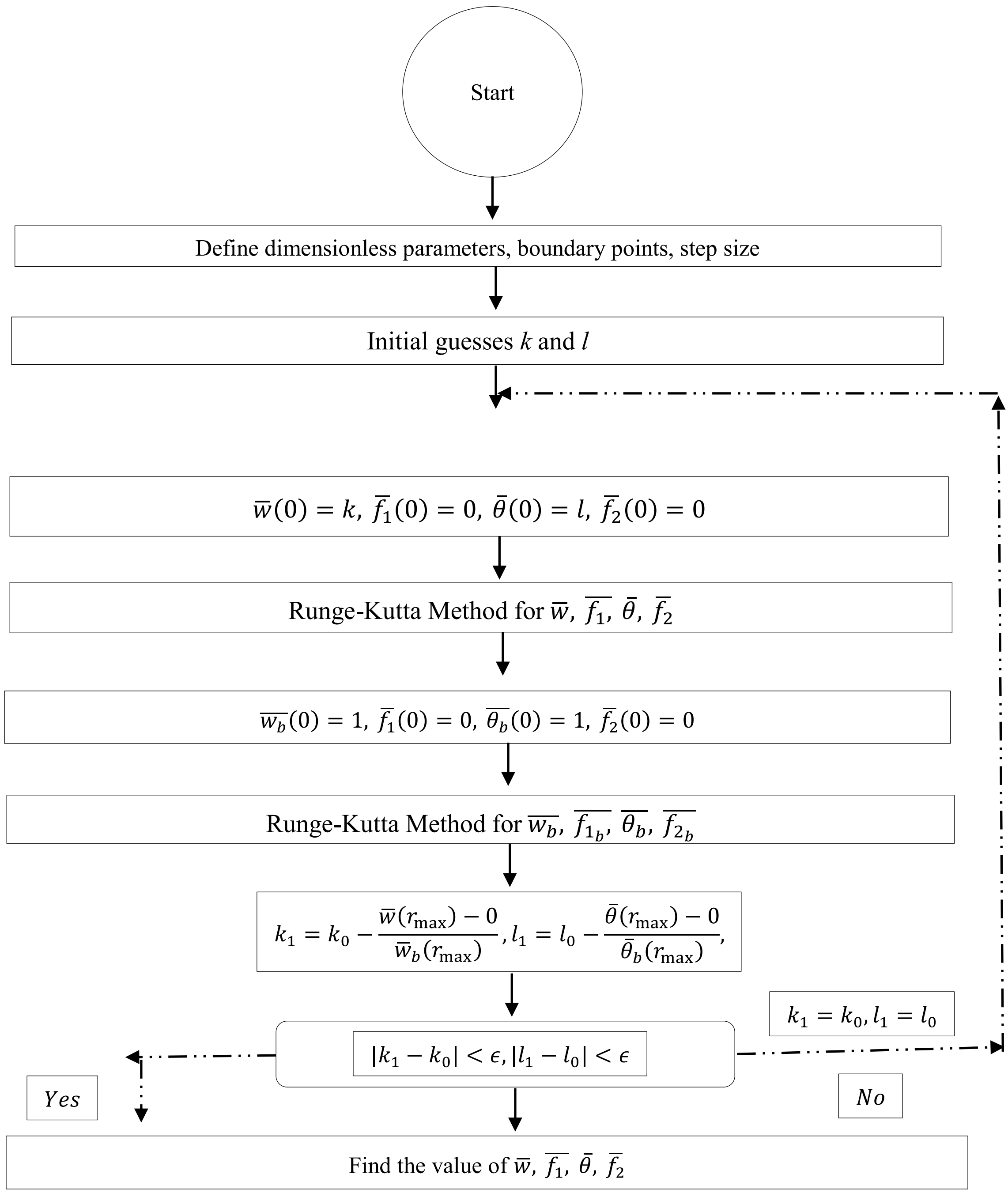

4 Results and discussion

In this portion, we intend to explore the obtained results. Here, we focused velocity $w(r)$ and temperature $\theta(r)$ through variation in some important parameters. The nonlinear boundary value problem is solved with the help of eminent shooting method based on Newton–Raphson method. Total eight figures are plotted in this section in which Figs. 2 and 3 are for constant case, Figs. 4, 5, 6 and 7 are for the case of temperature dependent viscosity (Reynolds and Vogel's model), and absolute errors between numerically computed velocity and temperature are depicted in Fig. 8. In each figure, left panel is for the velocity and right panel for the temperature profiles. Figure 2 predicts the effects of magnetic parameter M_e on velocity and temperature profiles, respectively. From the figure, it can be seen that the velocity and temperature profile decreases with increasing the values of magnetic parameter M_e. It is evident that when magnetic

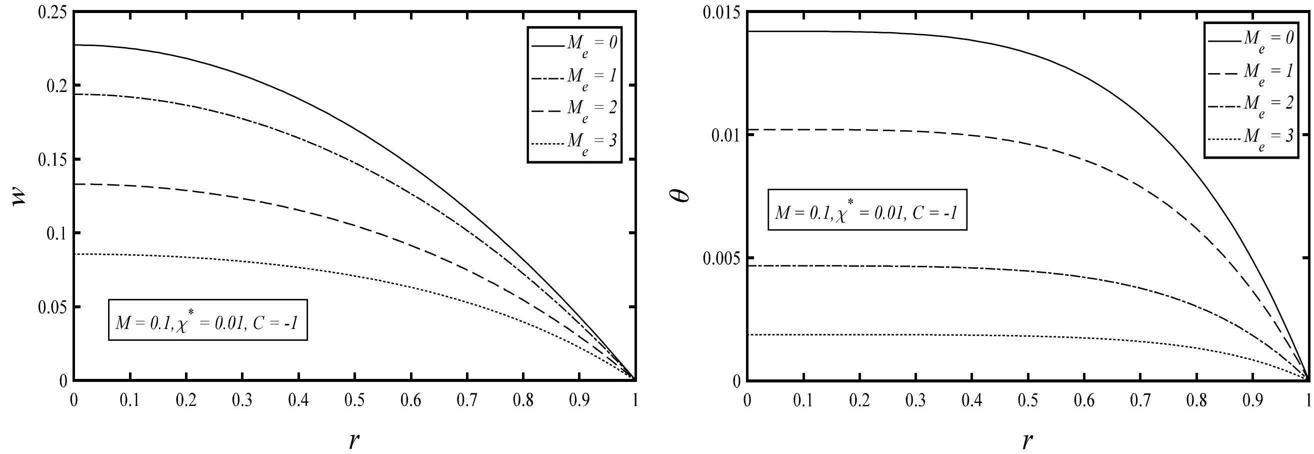

Fig. 2 Effects via M_e on w and θ

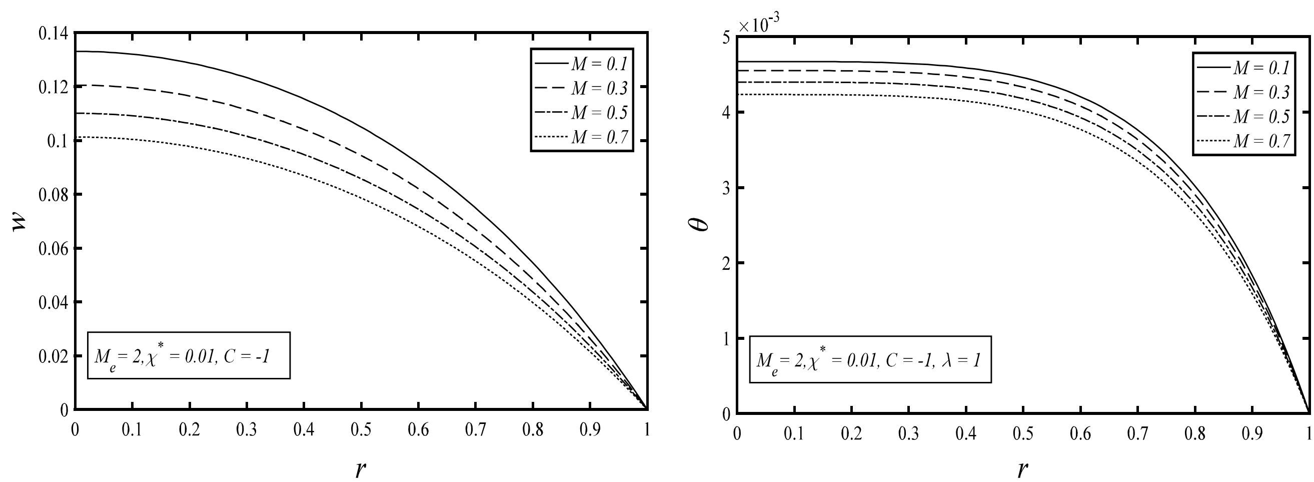

Fig. 3 Effects via M on w and θ

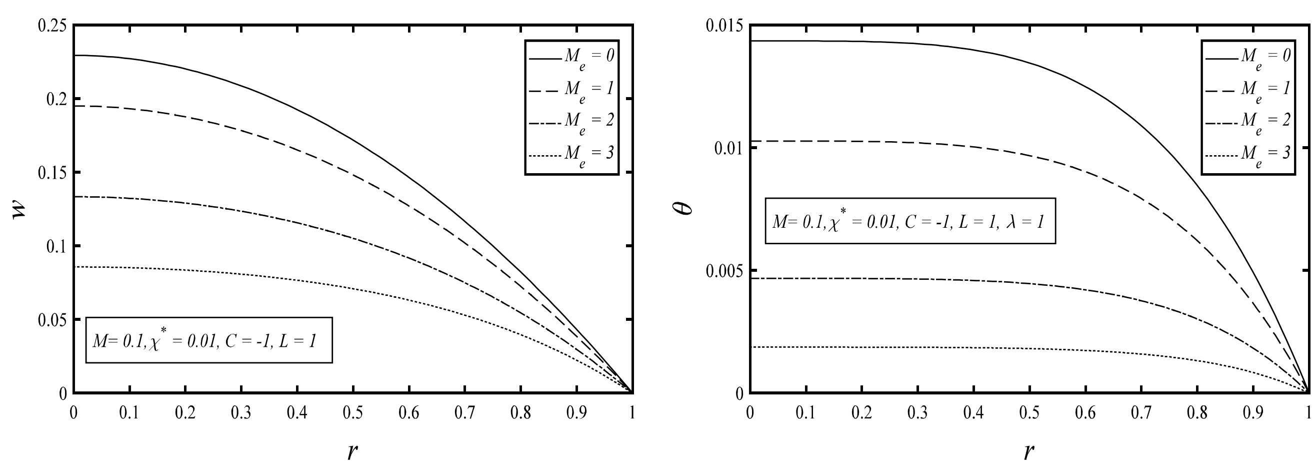

Fig. 4 Effects via M_e on w and θ

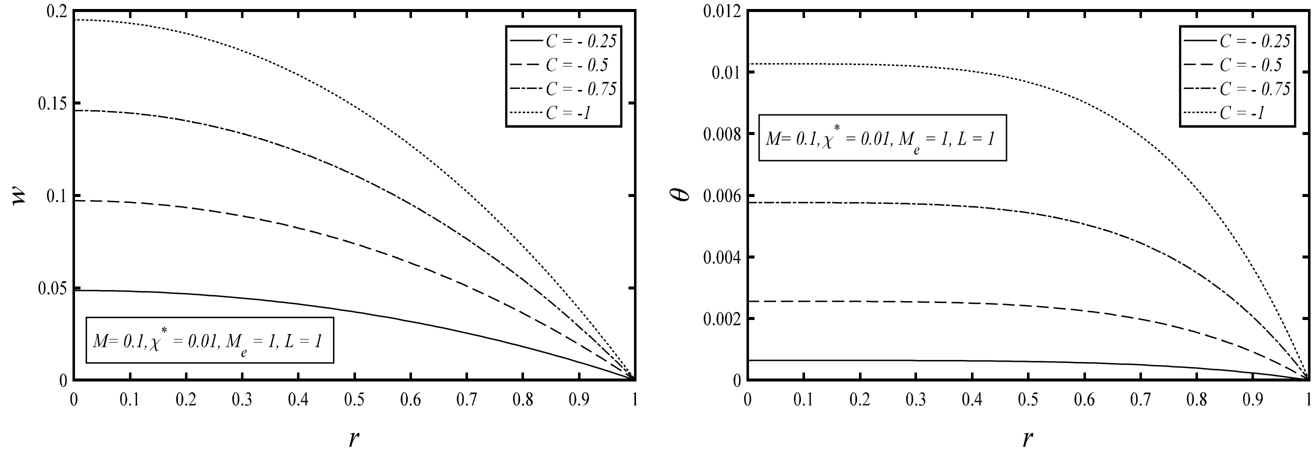

Fig. 5 Effects via C on w and θ

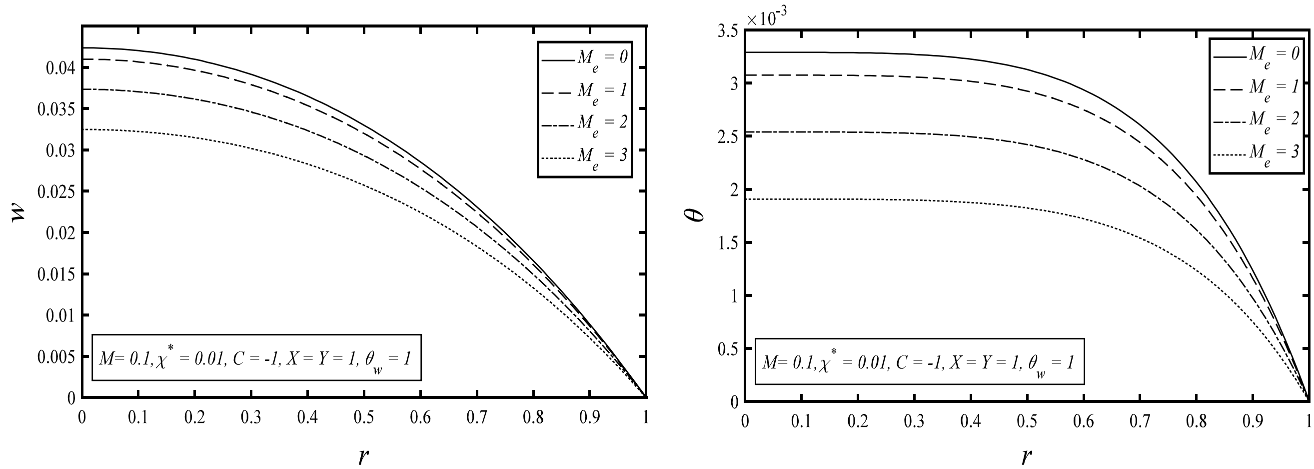

Fig. 6 Effects via M_e on w and θ

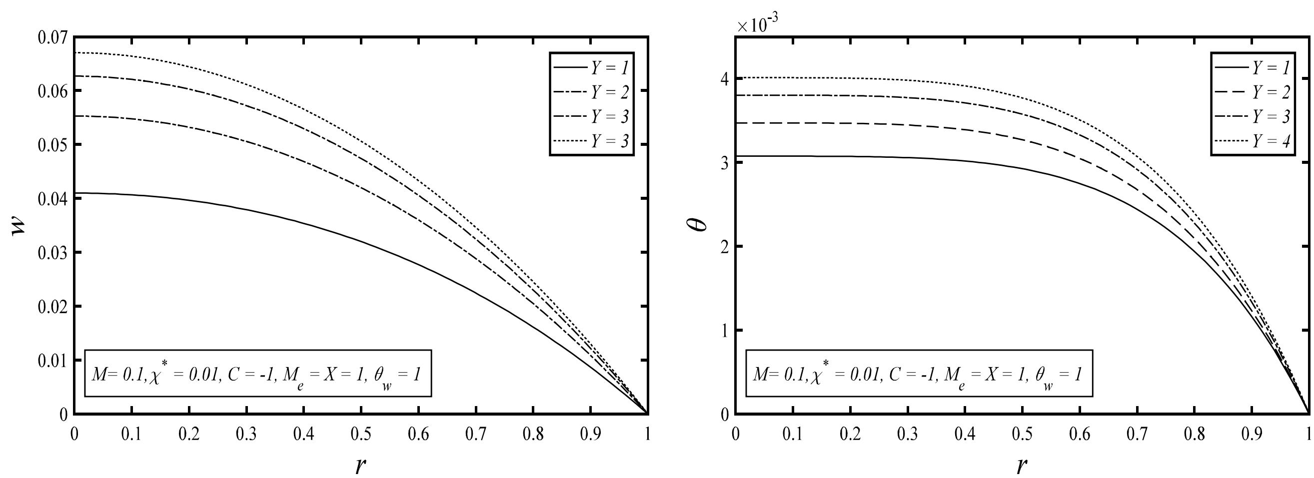

Fig. 7 Effects via Y on w and θ

forces or Lorentz forces (friction forces) are dominating over viscous forces as a result the velocity of the fluid is showing decreasing trend against magnetic parameter and boundary layer thickness is also decreases. Figure 3 illustrates the behavior of Eyring–Powell parameter M on velocity and temperature fields. It scrutinized that the velocity and temperature decays through M. Physically, for increasing the values of M, the viscosity of the fluid will decrease; therefore, the resistance in the fluid particle decreases and less heat is produced. The effects of magnetic parameter M_e on velocity

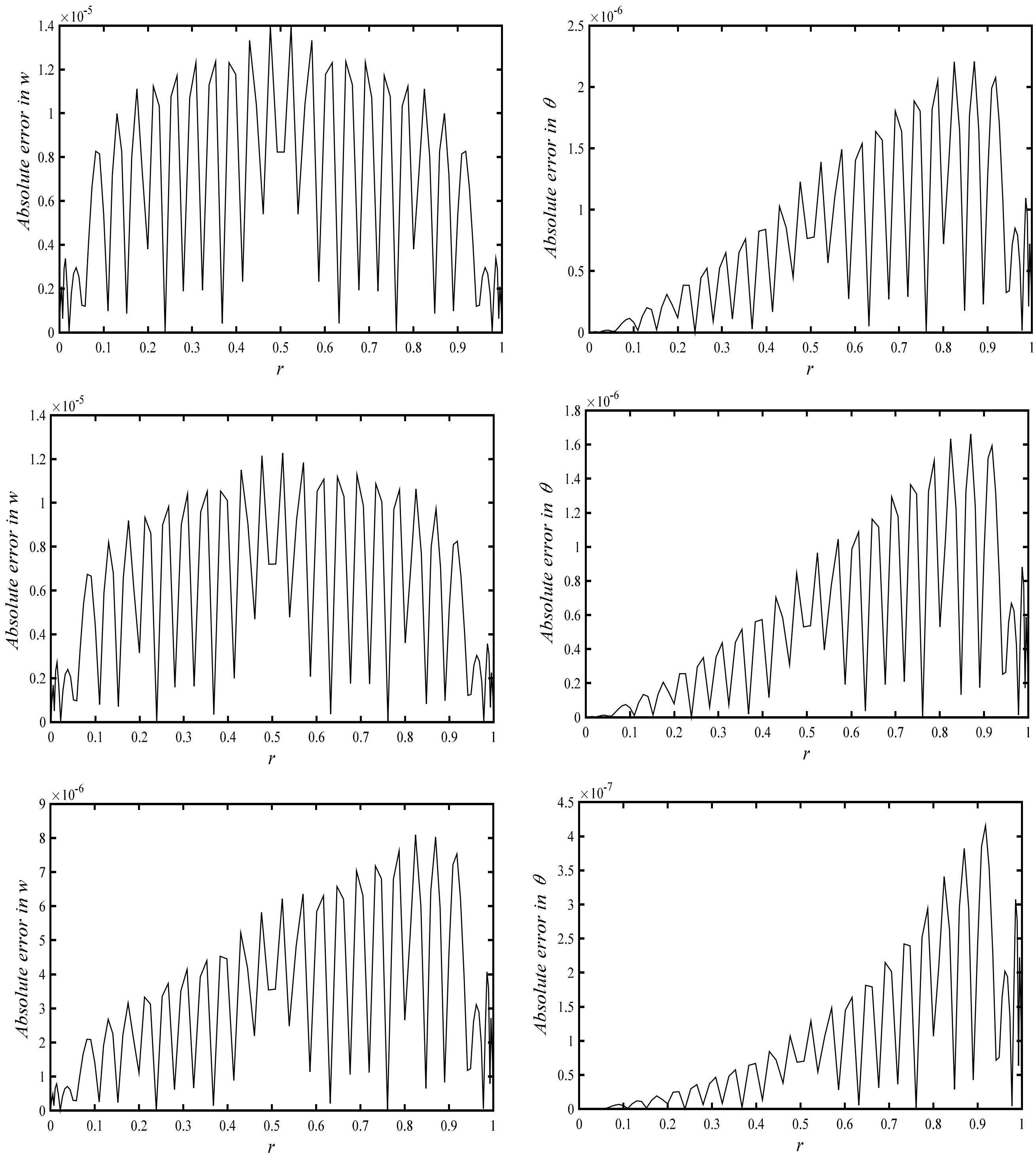

Fig. 8 Absolute error in velocity and temperature for $M_e = 1, 2, 3$

and temperature fields are highlighted in Fig. 4 for the case of Reynolds model. It is noted that the effects of magnetic parameter are similar as we have shown for the case of constant viscosity model. Basically, the velocity and temperature fields are decreasing function of magnetic parameter for both cases namely, constant and Reynods model cases. Figure 5 depicts the effects of pressure gradient on velocity and temperature profiles. It is clearly noted that both velocity and temperature profiles rises via magnitude of the pressure gradient. It is noted that when C becomes negative, the velocity of the fluid is going maximum at the center of the pipe physically which means that thickness of the velocity boundary layer decreases. Figure 6 illustrates the effects of M_e on $w(r)$ and $\theta(r)$ for the case of Vogel's model. It is clearly noted that the velocity and temperature profiles having similar trend against the values of magnetic parameter M_e as we discussed into previous two cases. The effects of parameter Y are presented in Fig. 7. The velocity and temperature fields are also increases with increasing the value of Y. To verify the numerical results obtained from shooting method, we solve numerically the same problem via pseudo-spectral collocation method for different cases. The absolute errors between numerically computed velocity and temperature are depicted in Fig. 8. The numerically values of velocity and temperature for $M_e = 1, 2, 3$ are four and five digits accurate comparing with pseudo-spectral collocation method.

5 Conclusions

The steady-state MHD Eyring–Powell fluid inside the infinite long pipe is discussed here through numerically. The coupled nonlinear ordinary differential equations arise from the mechanics of fluid. The simulations are constructed for both constant and variable viscosity models. The effects of some important parameters on velocity $w(r)$, and temperature $\theta(r)$ are noted with the help of plots. The major outcomes are listed below:

- The velocity and temperature fields are diminishing with increasing M_e in all cases, namely constant, Reynolds and Vogel's models.
- Both velocity and temperature profiles rise via magnitude of the pressure gradient and material parameter Y.
- The validity of our numerical results due to shooting method is presented by comparing them with the numerical results produced by pseudo-spectral collocation method. Relative absolute errors are plotted and achieved accuracies are of the order four and five in w and θ, respectively.

Compliance with ethical standards

Conflict of interest Authors have no conflict of interest regarding to this manuscript.

References

1. Pandey V, Holm S (2016) Linking the fractional derivative and the lomnitz creep law to non-Newtonian time-varying viscosity. Phys Rev E 94(3):032606
2. Bird RB, Dai GC, Yarusso BJ (1983) The rheology and flow of viscoplastic materials. Rev Chim Eng 1(1):1–70
3. Mahmood A, Parveen S, Ara A, Khan NA (2009) Exact analytic solutions for the unsteady flow of a non-Newtonian fluid between two cylinders with fractional derivative model. Commun Nonlinear Sci Numer Simul 14(8):3309–3319
4. Fielding SM (2007) Complex dynamics of shear banded flows. Soft Matter 3(10):1262–1279
5. Luikov AV, Shulman ZP, Puris BI (1969) External convective mass transfer in non-Newtonian fluid: Part I. Int J Heat Mass Transf 12(4):377–391
6. Li B, Zheng L, Zhang X (2011) Heat transfer in pseudo-plastic non-Newtonian fluids with variable thermal conductivity. Energy Convers Manage 52(1):355–358
7. Tapadia P, Wang SQ (2006) Direct visualization of continuous simple shear in non-Newtonian polymeric fluids. Phys Rev Lett 96(1):016001
8. Balmforth NJ, Frigaard IA, Ovarlez G (2014) Yielding to stress: recent developments in viscoplastic fluid mechanics. Annu Rev Fluid Mech 46:121–146
9. Pimenta TA, Campos J (2012) Friction losses of Newtonian and non-Newtonian fluids flowing in laminar regime in a helical coil. Exp Therm Fluid Sci 36:194–204
10. Akbar NS, Nadeem S, Changhoon L, Hayat KZ, Rizwan H (2013) Numerical study of Williamson nano fluid flow in an asymmetric channel. Results Phys 3:161–166
11. Akbar NS, Nadeem S (2012) Thermal and velocity slip effects on the peristaltic flow of a six constant Jeffrey's fluid model. Int J Heat Mass Trans 55:3964–3970
12. Ellahi R (2009) Effects of the slip boundary condition on non-Newtonian flows in a channel. Commun Nonlinear Sci Numer Simul 14:1377–1384
13. Nadeem S, Haq R, Lee C (2012) MHD flow of a Casson fluid over an exponentially shrinking sheet. Sci Iran 19:1550–1553
14. Alamri SZ, Khan AA, Azeez M, Ellahi R (2019) Effects of mass transfer on MHD second grade fluid towards stretching cylinder: a novel perspective of Cattaneo–Christov heat flux model. Phys Lett A 383:276–281
15. Bhatti MM, Zeeshan A, Ellahi R, Shit GC (2018) Mathematical modeling of heat and mass transfer effects on MHD peristaltic propulsion of two-phase flow through a Darcy–Brinkman–Forchheimer porous medium. Adv Powder Technol 29:1189–1197
16. Bhatti MM, Zeeshan A, Ijaz I, Ellahi R (2017) Heat transfer and inclined magnetic field analysis on peristaltically induced motion of small particles. J Braz Soc Mech Sci Eng 39(9):3259–3267
17. Ellahi R, Alamri SZ, Basit A, Majeed A (2018) Effects of MHD and slip on heat transfer boundary layer flow over a moving plate based on specific entropy generation. J Taibah Univ Sci 12(4):476–482
18. Hassan M, Marin M, Sharif AA, Ellahi R (2018) Convection heat transfer flow of nanofluid in a porous medium over wavy surface. Phys Lett A 382:2749–2753

19. Majeed A, Zeeshan A, Alamri SZ, Ellahi R (2018) Heat transfer analysis in ferromagnetic viscoelastic fluid flow over a stretching sheet with suction. Neural Comput Appl 30(6):1947–1955
20. Shirvan KM, Mamourian M, Mirzakhanlari S, Ellahi R, Vafai K (2017) Numerical investigation and sensitivity analysis of effective parameters on combined heat transfer performance in a porous solar cavity receiver by response surface methodology. Int J Heat Mass Transf 105:811–825
21. Hassan M, Marin M, Ellahi R, Alamri SZ (2018) Exploration of convective heat transfer and flow characteristics synthesis by Cu–Ag/water hybrid-nanofluids. Heat Transf Res 49(18):1837–1848
22. Yousif MA, Ismael HF, Abbas T, Ellahi R (2019) Numerical study of momentum and heat transfer of MHD Carreau nanofluid over exponentially stretched plate with internal heat source/sink and radiation. Heat Transf Res 50(7):649–658
23. Turkyilmazoglu T (2011) Thermal radiation effects on the time-dependent MHD permeable flow having variable viscosity. Int J Therm Sci 50:88–96
24. Turkyilmazoglu T (2012) Exact solutions to heat transfer in straight fins of varying exponential shape having temperature dependent properties. Int J Therm Sci 55:69–75
25. Bhatti MM, Zeeshan A, Ellahi R (2016) Heat transfer analysis on peristaltically induced motion of particle-fluid suspension with variable viscosity: clot blood model. Comput Methods Programs Biomed 137:115–124
26. Ellahi R, Riaz A (2010) Analytical solutions for MHD flow in a third-grade fluid with variable viscosity. Math Comput Model 52:1783–1793
27. Ellahi R (2013) The effects of MHD and temperature dependent viscosity on the flow of non-Newtonian nanofluid in a pipe: analytical solutions. Appl Math Modell 37:1451–1467
28. Hayyat T, Awais M, Asghar S (2013) Radiative effects in a three-dimensional flow of MHD Eyring–Powell fluid. J Egypt Math Soc 21:379–384
29. Hayat T, Khan MI, Waqas M, Alsaedi A (2017) Effectiveness of magnetic nanoparticles in radiative flow of Eyring–Powell fluid. J Mol Liq 231:126–133
30. Akbar NS, Ebaid A, Khan ZH (2015) Numerical analysis of magnetic field effects on Eyring–Powell fluid flow towards a stretching sheet. J Magn Magn Mater 382:355–358
31. Nadeem S, Saleem S (2014) Mixed convection flow of Eyring–Powell fluid along a rotating cone. Results Phys 4:54–62
32. Khan NA, Aziz S, Khan NA (2014) MHD flow of Powell-Eyring fluid over a rotating disk. J Taiwan Inst Chem E 45:2859–2867
33. Hayat T, Sajjad R, Muhammad T, Alsaedi A, Ellahi R (2017) On MHD nonlinear stretching flow of Powell-Eyring nanomaterial. Results Phys 7:535–543
34. Ellahi R, Shivanian E, Abbasbandy S, Hayat T (2016) Numerical study of magnetohydrodynamics generalized Couette flow of Eyring–Powell fluid with heat transfer and slip condition. Int J Numer Methods Heat Fluid Flow 26:1433–1445
35. Ali N, Nazeer F, Nazeer M (2018) Flow and heat transfer analysis of Eyring–Powell fluid in a pipe. Z Naturforsch A 73:265–274
36. Majeed A, Javed T, Ghaffari A (2017) A computational study of Brownian and thermophoresis effects on non-linear radiation in boundary layer flow of Maxwell nanofluid initiated due to elongating cylinder. Can J Phys 95:969–975
37. Hayat T, Iqbal Z, Qasim M, Alsaedi A (2013) Flow of an Eyring–Powell fluid with convective boundary conditions. J Mech 29:217–224
38. Powell RE, Erying H (1994) Mechanism for the relaxation theory of viscosity. Nature 154:427–428
39. Cebeci T, Keller HB (1971) Shooting and parallel shooting methods for solving the Falkner–Skan boundary layer equation. J Comput Phys 7:289–300
40. Nazeer M, Ahmad F, Saleem A, Saeed M, Naveed S, Shaheen M, Aidarous EA (2019) Effects of constant and space dependent viscosity on Eyring–Powell fluid in a pipe: comparison of perturbation and explicit finite difference method. Z Naturforsch A. https://doi.org/10.1515/zna-2019-0095
41. Nazeer M, Ali N, Javed T (2018) Numerical simulation of MHD flow of micropolar fluid inside a porous inclined cavity with uniform and non-uniform heated bottom wall. Can J Phys 96(6):576–593
42. Ali N, Nazeer M, Javed T, Siddiqui MA (2018) Buoyancy driven cavity flow of a micropolar fluid with variably heated bottom wall. Heat Trans Res 49(5):457–481
43. Nazeer M, Ali N, Javed T (2018) Effects of moving wall on the flow of micropolar fluid inside a right angle triangular cavity. Int J Numer Methods Heat Fluid Flow 28(10):2404–2422
44. Ali N, Nazeer M, Javed T, Abbas F (2018) A numerical study of micropolar flow inside a lid-driven triangular enclosure. Meccanica 53(13):3279–3299
45. Nazeer M, Ali N, Javed T (2018) Natural convection flow of micropolar fluid inside a porous square conduit: effects of magnetic field, heat generation/absorption, and thermal radiation. J Porous Med 21(10):953–975
46. Nazeer M, Ali N, Javed T, Asghar Z (2018) Natural convection through spherical particles of a micropolar fluid enclosed in a trapezoidal porous container. Eur Phys J Plus 133(10):423
47. Nazeer M, Ali N, Javed T (2019) Numerical simulations of MHD forced convection flow of micropolar fluid inside a right angle triangular cavity saturated with porous medium: effects of vertical moving wall. Can J Phys 97:1–13
48. Ali N, Nazeer M, Javed T, Razzaq M (2019) Finite element analysis of bi-viscosity fluid enclosed in a triangular cavity under thermal and magnetic effects. Eur Phys J Plus 134:2
49. Nazeer M, Ali N, Javed T, Razzaq M (2019) Finite element simulations based on Peclet number energy transfer in a lid-driven porous square container filled with micropolar fluid: impact of thermal boundary conditions. Int J Hydrog Energy 44:953–975
50. Nazeer M, Ali N, Javed T, Nazir MW (2019) Numerical analysis of full MHD model with Galerkin finite element method. Eur Phys J Plus 134:204